Tang *et al. BMC Medical Imaging* (2025) 25:82
https://doi.org/10.1186/s12880-025-01622-3

BMC Medical Imaging

RESEARCH

Open Access

Stapes footplate's posterior border protrudes the vestibule in healthy ears: anatomical insights from ultra-high-resolution CT

Ruowei Tang[1], Ning Xu[1], Zhengyu Zhang[1], Zhongrui Chen[2], Heyu Ding[1], Zhenghan Yang[1], Zhenchang Wang[1*] and Pengfei Zhao[1*]

Abstract

Background The stapes footplate (SF) and annular ligament (AL) in the oval window region are of paramount significances. This study aims to assess the visibility of AL and the relative positioning of the SF and vestibule using ultra-high-resolution computed tomography (U-HRCT).

Methods U-HRCT images between September 2020 and April 2023 were retrospectively reviewed, and 479 ears deemed healthy from both clinical and radiological perspectives were included. AL was considered visible when manifesting as linear low attenuation between the SF and oval window, and the visibility was assessed for its four borders (anterior, posterior, superior and inferior). Two neuroradiologists conducted measurements independently for the SF length, SF-oval window angle, and SF protrusion depth into the vestibule. The results were described on the entire cohort, and compared by age and by sex.

Results A cohort comprising 479 participants [median age 58 years (interquartile range 35–65); 269 females] with 479 healthy ears were included. The inferior border of the AL region demonstrated the highest visibility (476/479, 99.4%), whereas the posterior border exhibited the lowest visibility rate (394/479, 82.3%). The median protrusion depth of the SF posterior border into the vestibule was 0.4 mm (interquartile range 0.3–0.5 mm). Statistically significant differences were observed within age and sex groups for the SF length and the SF protrusion depth (all $P < 0.05$).

Conclusions This study established radiological features for the SF and AL in healthy ears through U-HRCT. The findings are essential for providing normative references, expediting disease diagnosis, and aiding in selection of surgical strategy.

Trial registration Retrospectively registered.

Keywords Oval window, Ear, Healthy volunteers, Tomography, X-Ray computed, Diagnostic techniques, Otological, Otologic surgical procedures

*Correspondence:
Zhenchang Wang
cjr.wzhch@vip.163.com
Pengfei Zhao
zhaopengf05@163.com
[1]Department of Radiology, Beijing Friendship Hospital, Capital Medical University, 95 Yong'an Road, Xicheng District, Beijing 100050, PR China
[2]Department of Otolaryngology and Head & Neck, Beijing Friendship Hospital, Capital Medical University, Beijing 100050, PR China

Background

The oval window region consists of the oval window, stapes, and the annular ligament (AL). Among these structures, the stapes footplate (SF) and AL are of paramount significances in sound conduction, drug delivery, force dynamics and disease diagnosis [1–3], which are closely related to the anatomical characteristics. For instance, in otosclerosis, the SF can exhibit either localized or diffuse thickening, reducing sound conduction efficiency [4–6]. The anatomic properties of the AL, a sandwich-beam connection between the SF and oval window, considerably influence stapedial stiffness and motion, especially in pathological conditions such as otosclerosis and congenital SF fixation [6, 7]. Thus, it is essential to define the normal anatomical morphology of the SF and AL as a reference for disease diagnosis. However, the limited availability of radiographic evidence arises from the difficulty in visualizing the SF and AL, given their extremely thin dimensions, often as fine as a hundred micrometers [8].

In the realm of imaging assessment, computed tomography (CT) serves various purposes in preoperative diagnosis, primarily concentrating on features like the height of oval window niche, the SF thickness [4], and volume or thickness of the AL [1]. However, there is a scarcity of CT studies that have evaluated the relative positioning of these important anatomic landmarks. Recent advancements in ultra-high-resolution computed tomography (U-HRCT) have significantly enhanced the visualization of delicate structures within the temporal bone, depicting normal anatomy and anatomical variations for structures such as the stapes [9] and chorda tympani nerve [10]. U-HRCT has also proven invaluable in providing radiological evidence for ear diseases such as otosclerosis [4, 11], facial nerve canal dehiscence [12], and cochlea new bone formation [13].

Therefore, the objectives of this study were twofold: (1) to assess the visibility of the AL and the relative positioning of the SF with the vestibule in healthy ears using U-HRCT, and (2) to investigate age- and sex-related differences in these radiographic features, providing insights into individual anatomical variations.

Methods

Study design

This single-center retrospective and observational study, performed at a tertiary referral center, was conducted in accordance with the local institutional review board (approval No. 2022-P2-055 and 2024-P2-061-02) and the declaration of Helsinki. Written informed consent was obtained from all participants included in this study. The evaluation included both qualitative and quantitative analyses encompassing: (1) visualization of the AL region for its four borders, (2) measurement of the SF and oval window lengths, SF-oval window angle and SF protrusion depth into the vestibule.

Eligible participants

Consecutive patients who underwent U-HRCT examination at our institution between September 2020 and April 2023 were initially included. Patients suspected of having otological related diseases (i.e., otitis media, cholesteatoma, otosclerosis, Meniere's disease or congenital malformation) underwent U-HRCT examination. As we aimed to study ears that were both radiologically and clinically healthy, the following exclusion criteria were applied in patients: (1) age under 18 years, (2) with presence of external auditory canal, middle ear, or inner ear diseases for both ears, (3) with abnormal clinical or imaging findings (audiometric, otoacoustic emissions, acoustic immittance, otoscopy or gadolinium-enhanced imaging) for both ears, (4) with incomplete clinical information, and (5) whose images demonstrated inadequate coverage or severe motion artifacts interfering with image interpretation (Fig. 1). All patients visited our hospital for otologic conditions; none underwent U-HRCT examination solely for the purpose of this study.

U-HRCT protocols

The temporal bones were scanned unilaterally with a U-HRCT scanner (Ultra3D, LargeV, Beijing) at 100–110 kVp, 120–180 mAs, and both temporal bones of each patient were scanned. The focal spot size of the X-ray source was 0.25 mm (IEC 60336) and the detector pixel size was 0.0748 mm × 0.0748 mm. The device incorporated a 35-mm collimation, a field of view of 65 mm, and a voxel size of 0.1 mm × 0.1 mm × 0.1 mm. The U-HRCT scanning generated isotropic voxels, enabling visualization of the temporal bone structures from any desired direction. The exposure dose ranged from 156 to 295 μGy m^2 for each scan.

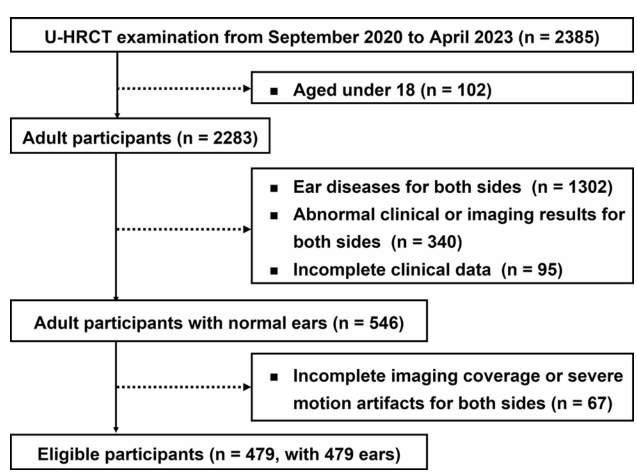

Fig. 1 Flow chart of the study

Imaging analysis

Standard observation orientation

Images of the included ears were displayed using an offline software (RadiAnt DICOM Viewer, 2020.2, Medixant, Poland). The standard observational plane, defined as the axial plane aligned parallel to the long axis of the stapes, was established through precise adjustments in the coronal and sagittal views. First, the sagittal position line was adjusted parallel to the tympanic facial nerve canal's long axis. Then, in the coronal plane, the slice through the SF center was selected, and the axial position line was reoriented vertical to the tympanic membrane. With these adjustments, the standard axial, sagittal, and coronal planes were conclusively established.

Visibility of the AL region

The visibility of the AL region was assessed for its four borders: anterior, posterior, superior, and inferior. All axial and coronal slices featuring the SF were utilized to assess the visibility of the anterior/posterior and superior/inferior AL borders, respectively. (Fig. 2). The AL was considered visible when it appeared as a linear low-attenuation on any of these slices (Fig. 3). Visibility of the AL region was determined by 2 dedicated neuroradiologists (R. T. and N. X.) with 8 and 4 years of experience in reviewing head and neck imaging. In cases of discrepancies, the two observers reached a consensus.

Quantitative analysis of SF and oval window position

The measurements were conducted by the two independent neuroradiologists manually, who were blinded to the participants' clinical data. The images were randomized, and measurements were conducted on the axial image at the SF center with the following steps. (1) Four reference points were selected: the anterior and posterior borders of the SF, and the anterior and posterior bony ridges of the oval window. The distances between the anterior and posterior ridges of the SF and oval window were defined as their lengths, respectively (Fig. 4). (2) To define the positional relationship of the SF and vestibule, an additional point of the SF that extended most inward into the vestibule (SF_{medial}) was chosen. Two lines, one connecting SF_{medial} to the anterior ridge of the oval window ($L_{SF-oval\ window}$) and the other linking the anterior and posterior ridges of the oval window ($L_{oval\ window}$), were delineated. The relative positioning was determined by the angle formed by $L_{SF-oval\ window}$ and $L_{oval\ window}$ (as SF-oval window angle) and the distance between the SF_{medial} and $L_{oval\ window}$ (as SF protrusion depth) (Fig. 4).

Statistical analysis

Statistical analyses were performed using SPSS software (version 26.0, IBM SPSS). The qualitative data were expressed using numbers (percentages), and the quantitative data were presented as median (interquartile range, IQR) due to their abnormal distribution. Interobserver's absolute agreement for quantitative measurements (distance and angle) was assessed using the two-way random intraclass correlation coefficient (ICC) with a 95% confidence interval (CI) based on the average values from both observers. The ICC values were interpreted as follows: poor < 0.50, moderate 0.50–0.75, good 0.75–0.90, and excellent > 0.90.

In addition, data were reported for the entire sample and compared by age (≤ 65 years vs. >65 years) and by sex (female vs. male). To compare inter-group difference for the visibility of AL posterior border, the Pearson chi-squared test was used. Specifically, the Fisher's exact was used for the anterior, superior and inferior border visibilities in the age and sex comparisons due to unbalanced categories. For example, only 9 (2.5%) and 2 (1.7%)

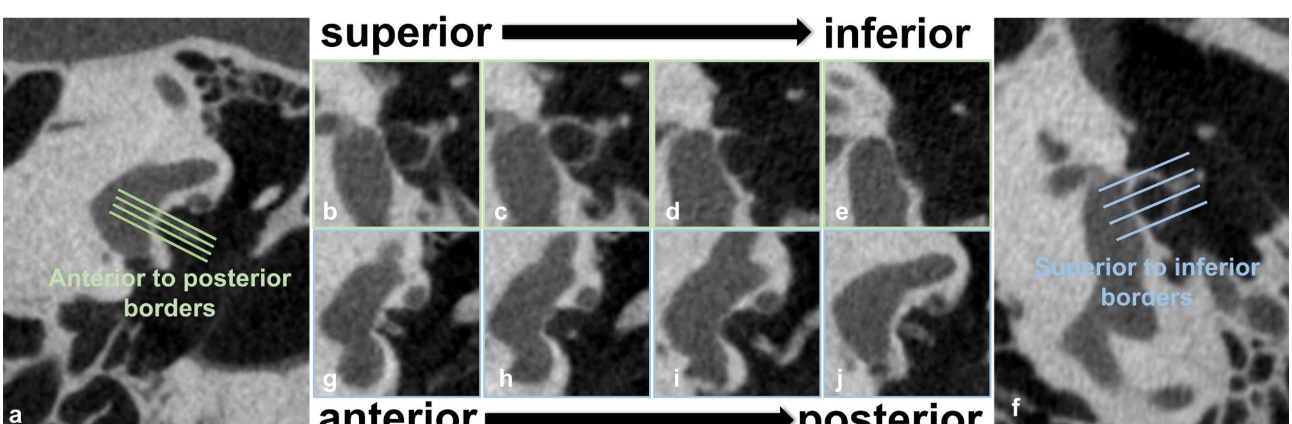

Fig. 2 Standard observation planes and slices for evaluation of the annular ligament. Visibility of the anterior and posterior borders are evaluated from axial images (green lines in **a**, as appeared in **b**-**e**), while the superior and inferior borders are assessed on coronal images (blue lines in **f**, as manifested in **g**-**j**)

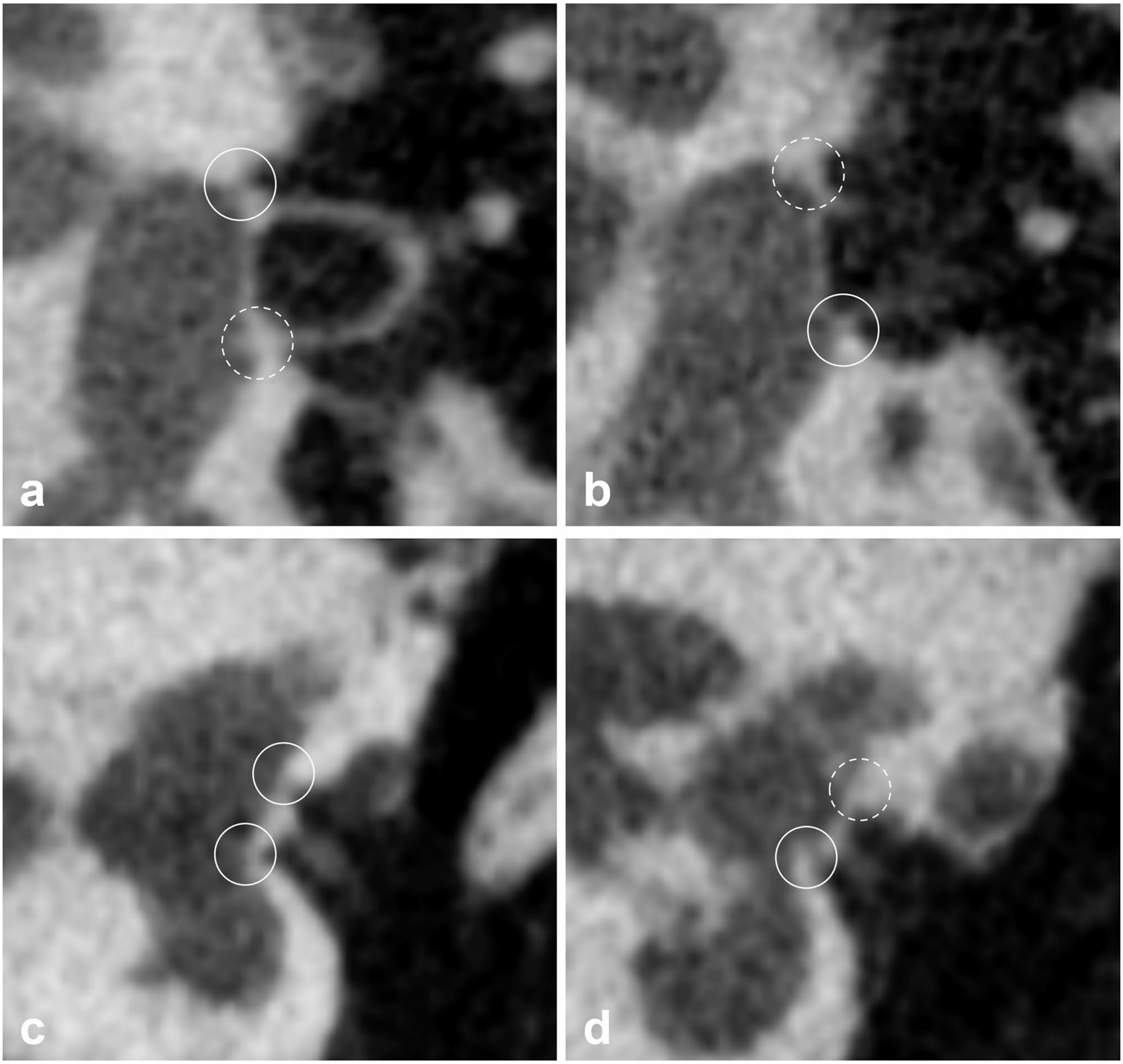

Fig. 3 Visibility of the annular ligament (AL) region for anterior and posterior (**a**-**b**) and superior and inferior (**c**-**d**) borders, with the solid circle indicating the visible area of the AL region and the dashed circle indicating the invisible area

anterior borders were not visible in the ≤65 years and >65 age groups, respectively, while the remaining 354 (97.5%) and 114 (98.3%) anterior borders were visible in these groups, respectively. The Mann-Whitney test was used for comparing quantitative data (distance and angle). Statistical significance was set at $P < 0.05$.

Results

Characteristics of eligible participants

A total of 479 participants (median 58 years, IQR 35–65 years, range 18–88 years; 269 female participants, 56.2%) with 479 healthy ears were finally included in the study (Table 1). That is, the analysis was performed for one ear per participant. The clinical and imaging results were normal for all included ears.

Interobserver agreement

The ICCs for quantitative measurements were all excellent with the values of 0.94 (95% CI 0.93–0.95) for the SF and oval window lengths, 0.96 (95% CI 0.95–0.97) for the SF-oval window angle, and 0.93 (95% CI 0.91–0.94) for the SF protrusion depth (Table 2).

Visibility of the AL region

Among the four borders, the inferior border of the AL had the highest visibility, recognized in 99.4% (476/479)

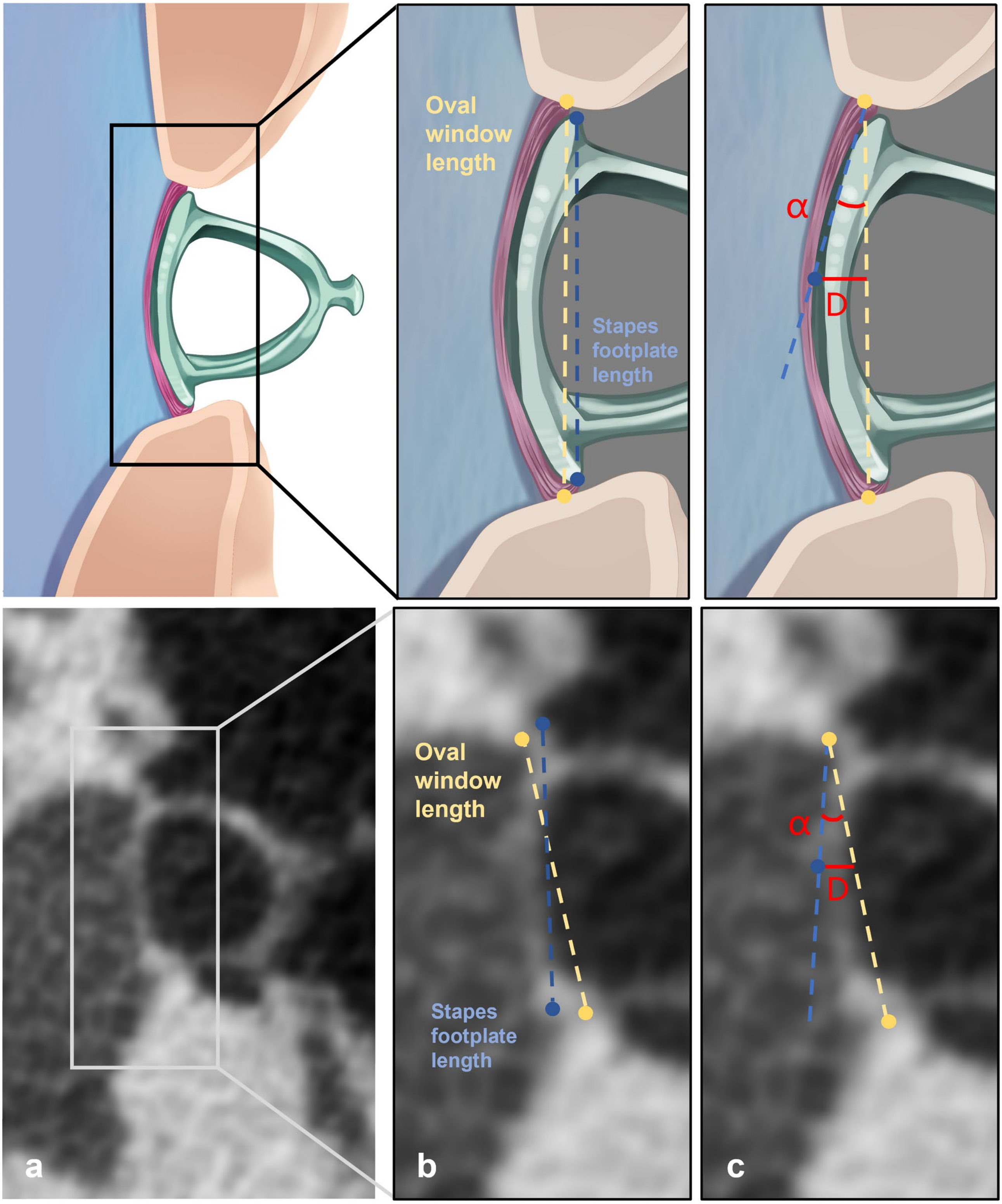

Fig. 4 Schematics (upper row) and U-HRCT images (lower row) illustrating distance and angle measurement. (**a**) oval window region, while b and c are the magnified images. (**b**) lengths of the stapes footplate (SF, blue) and oval window (yellow). (**c**) the SF-vestibule angle (α) formed by the line connecting the most medial point of SF (SF_{medial}) and the anterior bony ridge of the oval window ($L_{SF-oval\ window}$, blue line) and the line connecting the anterior and posterior bony edges of the oval window ($L_{oval\ window}$, yellow line). The SF protrusion depth (**D**) is defined as the distance between SF_{medial} and $L_{oval\ window}$

Table 1 Demographic and clinical data of the participants

Variable	Value
Age (y)	
Mean ± SD	51.9 ± 17.3
Median (IQR)	58 (35, 65)
Range	18–88
Sex, n (%)	
Female	269 (56.2)
Male	210 (43.8)
Side, n (%)	
Left	235 (49.1)
Right	244 (50.9)

SD = standard deviation; IQR = interquartile range

Table 2 Interobserver's absolute agreement for quantitative measurement of the oval window region

Quantitative measurement	Observer 1	Observer 2	ICC	95% CI
Oval window length (mm)	2.8 (2.7, 3.0)	2.9 (2.7, 3.0)	0.94	0.93–0.95
Stapes footplate length (mm)	2.7 (2.6, 2.9)	2.7 (2.5, 2.9)	0.94	0.93–0.95
Stapes footplate-oval window angle (°)	11.7 (9.3, 15.2)	12.2 (9.2, 15.2)	0.96	0.95–0.97
Stapes footplate protrusion depth (mm)	0.4 (0.3, 0.5)	0.4 (0.3, 0.5)	0.93	0.91–0.94

ICC = intraclass correlation coefficient; CI = confidence interval

cases, while the posterior border had the lowest visualization rate at 82.3% (394/479). Visibility for the superior border was 99.2% (475/479), whereas the anterior border presented a slightly lower visibility rate of 97.7% (468/479).

Positional relationship of the SF and vestibule

The SF length had a median value of 2.7 mm (IQR 2.6 mm, 2.9 mm) and the median oval window length was 2.9 mm (IQR 2.7 mm, 3.0 mm), with a minimal and maximal value of 2.3 mm and 3.6 mm, respectively. The posterior border of the SF protruded the vestibule with a median depth of 0.4 mm (IQR 0.3 mm, 0.5 mm) (Fig. 5), with a minimal value of 0.1 mm and a maximal value of 1.2 mm. The median SF-oval window angle was 12.1° (IQR 9.4°, 15.3°).

Age- and sex-specific differences

Visibilities for the AL borders (anterior, posterior, superior and inferior) were consistent between age groups (≤ 65 years vs. >65 years) and between females vs. males (all $P > 0.05$, Table 3).

For quantitative data, significant differences were observed between participants aged ≤ 65 years and > 65 years. The former group showed greater SF length [2.7 mm (IQR 2.6 mm, 2.9 mm) vs. 2.6 mm (IQR 2.5 mm, 2.8 mm), $P = 0.002$], oval window length [2.7 mm (IQR 2.6 mm, 2.9 mm) vs. 2.7 mm (IQR 2.5 mm, 2.8 mm), $P < 0.001$], and SF protrusion depth [0.4 mm (IQR 0.3 mm, 0.5 mm) vs. 0.4 mm (IQR 0.3 mm, 0.4 mm), $P = 0.001$] (Table 4).

In terms of sex-specific comparison, males overall showed larger values than females. For example, males

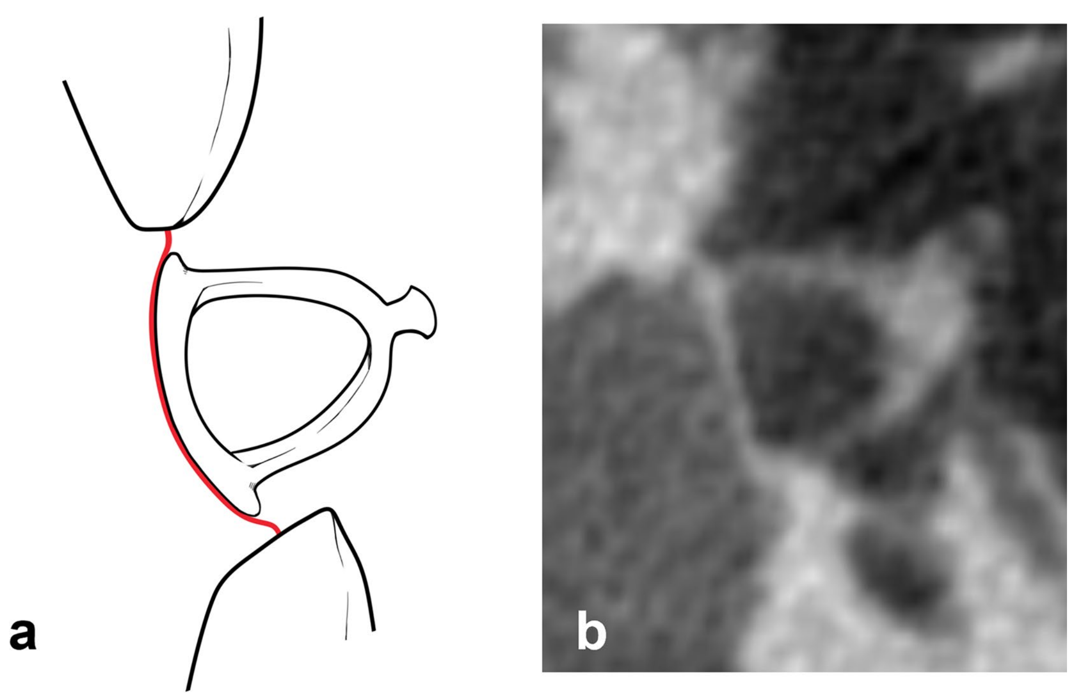

Fig. 5 The posterior border of the stapes footplate protruding the vestibule, as illustrated in the schematic diagram (**a**) and U-HRCT image (**b**)

Table 3 Qualitative features of the oval window region within the entire patient and group-wise comparison

Visibility for AL border, *n* (%)	Overall (*n* = 479)	Age				Sex			
		≤ 65 years (*n* = 363)	>65 years (*n* = 116)	χ^2	*P* value	Female (*n* = 269)	Male (*n* = 210)	χ^2	*P* value
Anterior border	468 (97.7)	354 (97.5)	114 (98.3)	-	0.636*	262 (97.4)	206 (98.1)	-	0.763*
Posterior border	394 (82.3)	292 (80.4)	102 (87.9)	3.379	0.066	220 (81.8)	174 (82.9)	0.093	0.760
Superior border	475 (99.2)	360 (99.2)	115 (99.1)	-	1.000*	266 (98.9)	209 (99.5)	-	0.635*
Inferior border	476 (99.4)	360 (99.2)	116 (100.0)	-	1.000*	266 (98.9)	210 (100.0)	-	0.260*

*The Fisher exact test is used for comparison of the anterior, superior and inferior border visibilities due unbalanced categories, and comparison of the posterior border is performed using the Pearson chi-squared test

Table 4 Quantitative features of the oval window region within the entire patient and group-wise comparison

Measurement of distance and angle, median (IQR)	Overall (*n* = 479)	Age				Sex			
		≤ 65 years (*n* = 363)	> 65 years (*n* = 116)	U	*P* value	Female (*n* = 269)	Male (*n* = 210)	U	*P* value
Oval window length (mm)	2.9 (2.7, 3.0)	2.7 (2.6, 2.9)	2.7 (2.5, 2.8)	16019.0	< 0.001	2.8 (2.7, 3.0)	2.9 (2.8, 3.1)	34375.5	< 0.001
Stapes footplate length (mm)	2.7 (2.6, 2.9)	2.7 (2.6, 2.9)	2.6 (2.5, 2.8)	16974.0	0.002	2.7 (2.5, 2.8)	2.8 (2.6, 2.9)	33531.5	< 0.001
Stapes footplate-oval window angle (°)	12.1 (9.4, 15.3)	12.1 (9.4, 15.3)	11.8 (9.4, 14.6)	20346.0	0.585	11.8 (9.5, 14.8)	12.3 (9.3, 15.8)	26759.5	0.323
Stapes footplate protrusion depth (mm)	0.4 (0.3, 0.5)	0.4 (0.3, 0.5)	0.4 (0.3, 0.4)	16664.0	0.001	0.4 (0.3, 0.5)	0.4 (0.3, 0.5)	31275.0	0.043

The analyses are performed using the Mann-Whitney test; IQR = interquartile range

had a longer oval window length [2.9 mm (IQR 2.8 mm, 3.1 mm) vs. 2.8 mm (IQR 2.7 mm, 3.0 mm), $P < 0.001$], a longer SF length [2.8 mm (IQR 2.6 mm, 2.9 mm) vs. 2.7 mm (IQR 2.5 mm, 2.8 mm), $P < 0.001$] and a deeper SF protrusion into the vestibule [0.4 mm (IQR 0.3 mm, 0.5 mm) vs. 0.4 mm (IQR 0.3 mm, 0.5 mm), $P = 0.043$], but the SF-oval window angle was not significantly different between males and females ($P = 0.323$) (Table 4).

Discussion

The SF and AL are crucial for sound conduction, drug delivery, force dynamics, and disease diagnosis [1–3], all of which are related to their anatomical features. In the present study of 479 healthy ears using U-HRCT, we found that 17.7% of the posterior AL border might not be visible in healthy ears, and the posterior border of SF protruded into the vestibule with a median depth of 0.4 mm. These findings can provide a normal anatomical reference for the oval window region, aid in disease diagnosis, and inform surgical strategy decisions.

The stapes, as the auditory ossicle connecting the incus and vestibule, has significant pathophysiological importance along with the AL region [1–3, 14, 15]. The mechanical properties of the AL region affect stapes vibration and sound conduction efficiency under physiological and pathological conditions, such as otosclerosis [1–3]. Histological studies have shown that the posterior and superior borders of the normal AL are firmly fixed, whereas the anterior and inferior borders are more relaxed, permitting mobility of the SF in these directions [16]. This finding aligns with the present study where U-HRCT showed the highest visibility at the inferior border and the lowest at the posterior border. Diagnosing AL diseases necessitates discretion to differentiate them from the pathological conditions, considering specific signs proposed from previous studies [5, 6].

In this study, we defined standard observation plane to observe the oval window region. The tympanic segment of the facial nerve and the tympanic membrane were considered the reference anatomic landmarks. Although the facial nerve might course tortuously in the axial orientation, the sagittal position line was placed between the semicanal of the tensor tympani and the pyramidal eminence. That is, the sagittal plane was determined by positions of these two landmarks, regardless of the nerve tract in between. Likewise, although the tympanic membrane changes position depending on the middle ear/external ear pressure, the position line was placed connecting the superior and inferior ridges of the tympanic annulus, remaining unaffected by the invagination of the tympanic membrane. In addition, the excellent interobserver agreement for quantitative measurements supported the idea to use these two landmarks to define a reliable standard observation plane for assessing the oval window region.

In contrast to previous studies where the optimal insertion depth of the piston in stapedotomy surgery ranged from 0.5 to 1.0 mm [17–20], the present study found the median protrusion depth in healthy ears was 0.4 mm. The normal positioning of the SF within the vestibule, without inducing symptoms such as hearing loss or vertigo, suggests a need for reassessing the conventional insertion depth of piston. It is reasonable to postulate that the insertion of piston might be optimal when simulating the exact natural position of the stapes. Therefore, surgeons should be aware of the anatomical diversity and evaluate the SF-oval window relationship when making treatment plans, especially concerning piston length. Another possible explanation for this finding is that although SF protruded the vestibule, the AL tissue sealed the posterior border, preventing the SF from penetrating into the inner ear and thereby sparing patients from the associated symptoms.

The U-HRCT device used in this study exhibits a significantly augmented spatial resolution when contrasted with high-resolution CT, which improves the display rate of delicate temporal bone structures in healthy controls [10] and patients with ear diseases [6, 11–13]. Specifically, visualization of the AL region requires heightened CT resolution, a criterion met by U-HRCT with its 0.1 mm resolution. AL on CT images presents as a linear low attenuation between the SF and bony edge of the oval window [5, 21]. On U-HRCT images, the display rates were all exceeding 82% for its four borders. Reports on the thickness of AL using micro-CT have been documented [1]; however, the practical application of micro-CT in clinical settingis limited to imaging specimens only [18]. Therefore currently, U-HRCT remains the best option for clinical practice in AL visualization, and quantitative analysis of the AL should be conducted in future studies.

Through group-wise comparison, the SF length, oval window length and the SF protrusion depth showed anatomical variations by age and sex. Although conventional views suggest that temporal bone structures are fully developed post-birth, age-specific differences of normal temporal bone have been reported for the external ear [22], mastoid air cell volume [23], sutures and fissures [24], Eustachian tube [25], and mastoid thickness [26]. All these differences might be influential factors for anatomical features of the oval window region. Age-related differences may also be correlated to the decrease in the number of vestibular ganglion cells in the saccule and utricle, which commences around the age of 60 years [27, 28]. These physiological changes could result in a gradual reduction of vestibular size, consequently impacting the morphology of the SF and oval window. For the sex-specific changes, male cranium increases in size after the age of 14 years and generally have larger temporal bone than females [23, 24, 29]. The noted differences may be associated with factors such as population size, eligible participant selection, and the methodology employed in measuring the sexual dimorphism [30]. Overall, age- and sex-related anatomic variations in oval window region should be considered during individualized assessment, especially for patients in need of stapedotomy treatment.

There are several limitations of this study. First, it cannot be guaranteed that the included study cohort had not experienced short-term otological symptoms such as mild otitis externa. However, the stringent inclusion and exclusion criteria minimized the risk, and no participants reported such symptoms for included ears. Second, to establish normative values for the oval window region in live, healthy ears, anatomical dissection was not performed as the reference standard. Nonetheless, CT is a crucial non-invasive method for imaging the temporal bone, and the radiographic measurements by CT exhibit equivalency with in situ measurement [31]. Third, this study did not include patients who underwent stapes surgery. In the future, including such patients will allow for a more comprehensive assessment on how preoperative and personalized analysis of natural stapes positioning can influence therapeutic outcomes. Last, since patients with bilateral ear diseases were excluded and only one healthy ear per patient was evaluated, no bilateral assessment was done, which could introduce some individual bias.

Conclusions

In conclusion, this study established the normative reference for AL visibility and the positional relationship of the SF and oval window in healthy ears using U-HRCT. A certain proportion of the posterior border of AL was not visible, and the posterior border of SF protruded into the vestibule. Differences related to age and sex were also observed. These findings are crucial for improving disease diagnosis and guiding surgical strategies, especially for patients requiring surgical treatment in the oval window region.

Abbreviations

AL	Annular ligament
CI	Confidence interval
CT	Computed tomography
ICC	Intraclass correlation coefficient
IQR	Interquartile range
SF	Stapes footplate
U-HRCT	Ultra-high-resolution computed tomography

Acknowledgements

Not applicable.

Author contributions

Conceptualization: R.T., N.X., Z.Z., Z.Y., Z.W., P.Z.; Methodology: H.D.; Formal analysis and investigation: R.T., N.X., Z.Z.; Writing—original draft preparation: R.T., N.X.; Writing—review and editing: R.T., N.X., Z.Z., Z.C., H.D.; Funding acquisition: R.T., Z.W., P.Z.; Resources: Z.Y., Z.W., P.Z.; Supervision: Z.W., P.Z.

Funding

This study has received funding by National Natural Science Foundation of China (No. 82302282, Ruowei Tang; No. 61931013, Zhenchang Wang; No. 82171886, Pengfei Zhao), Beijing Friendship Hospital, Capital Medical University (No. YYZZ202336), Beijing Natural Science Foundation (No. 7222301, Pengfei Zhao), Capital's Funds for Health Improvement and Research (No. 2022-1-1111, Zhenchang Wang), Beijing Scholar 2015 (No. [2015] 160, Zhenchang Wang), Beijing Key Clinical Discipline Funding (No. 2021-135, Zhenchang Wang).

Data availability
The datasets used and/or analysed during the current study are available from the corresponding author on reasonable request.

Declarations

Ethics approval and consent to participate
This single-center retrospective and observational study, performed at Beijing Friendship Hospital, Capital Medical University, was in accordance with the local institutional review board (approval No. 2022-P2-055 and 2024-P2-061-02) and the declaration of Helsinki.

Informed consent
Written informed consent was obtained from all participants included in this study.

Consent for publication
Not applicable.

Competing interests
The authors declare no competing interests.

Received: 28 November 2024 / Accepted: 27 February 2025
Published online: 07 March 2025

References

1. Mohammadi A, Jufas N, Sale P, Lee K, Patel N, O'Leary S. Micro-CT analysis of the anatomical characteristics of the stapedial annular ligament. Anat Sci Int. 2017;92(2):262–6.
2. Yang S, Xu D, Liu X. Evaluation of round window stimulation performance in otosclerosis using finite element modeling. Comput Math Methods Med. 2016;2016:3603207.
3. Muller C, Zahnert T, Ossmann S, Neudert M, Bornitz M. Vibroplasty combined with tympanic membrane reconstruction in middle ear ventilation disorders. Hear Res. 2019;378:166–75.
4. Akazawa Y, Ganaha A, Higa T, Kondo S, Oyakawa Y, Hirakawa H, Suzuki M, Yamashiro T. Measurement of stapes footplate thickness in otosclerosis by ultra-high-resolution computed tomography. Acta Otolaryngol. 2020;140(11):899–903.
5. Brown LA, Mocan BO, Redleaf MI. Diagnostic protocol for detecting otosclerosis on high-resolution temporal bone CT. Ann Otol Rhinol Laryngol. 2019;128(11):1054–60.
6. Tang R, Li J, Zhao P, Zhang Z, Yin H, Ding H, Xu N, Yang Z, Wang Z. Utility of machine learning for identifying stapes fixation on ultra-high-resolution CT. Jpn J Radiol. 2024;42(1):69–77.
7. Totten DJ, Marinelli JP, Carlson ML. Incidence of congenital stapes footplate fixation since 1970: A population-based study. Otol Neurotol. 2020;41(4):489–93.
8. Schar M, Dobrev I, Chatzimichalis M, Roosli C, Sim JH. Multiphoton imaging for morphometry of the sandwich-beam structure of the human stapedial annular ligament. Hear Res. 2019;378:63–74.
9. Tang R, Yin H, Wang Z, Zhang Z, Zhao L, Zhang P, Li J, Zhao P, Lv H, Zhang L, et al. Stapes visualization by ultra-high resolution CT in cadaveric heads: A preliminary study. Eur J Radiol. 2021;141:109786.
10. Tang R, Zhang Z, Zhao L, Xu N, Wu Q, Xie J, Zhao P, Yin H, Yang Z, Wang Z. Radiological evaluation of tympanic segment of Chorda tympani nerve in normal ears: an Ultra-High-Resolution computed tomography study. World Neurosurg. 2022;168:e34–42.
11. Xu N, Ding H, Tang R, Li X, Zhang Z, Lv H, Dai C, Qiu X, Huang Y, Han X, et al. Comparative study of the sensitivity of ultra-high-resolution CT and high-resolution CT in the diagnosis of isolated fenestral otosclerosis. Insights Imaging. 2023;14(1):211.
12. Tang R, Zhang Z, Zhao P, Zhao L, Xu N, Yin H, Yang Z, Wang Z. A novel imaging scoring method for identifying facial Canal dehiscence: an ultra-high-resolution CT study. Eur Radiol. 2023;33(4):2830–9.
13. Heutink F, Klabbers TM, Huinck WJ, Lucev F, van der Woude WJ, Mylanus EAM, Verbist BM. Ultra-high-resolution CT to detect intracochlear new bone formation after cochlear implantation. Radiology. 2022;302(3):605–12.
14. Salt AN, King EB, Hartsock JJ, Gill RM, O'Leary SJ. Marker entry into vestibular Perilymph via the stapes following applications to the round window niche of guinea pigs. Hear Res. 2012;283(1–2):14–23.
15. King EB, Salt AN, Eastwood HT, O'Leary SJ. Direct entry of gadolinium into the vestibule following intratympanic applications in Guinea pigs and the influence of cochlear implantation. J Assoc Res Otolaryngol. 2011;12(6):741–51.
16. Marquet J. The incudo-malleal joint. J Laryngol Otol. 1981;95(6):543–65.
17. Huttenbrink KB. Biomechanics of stapesplasty: a review. Otol Neurotol. 2003;24(4):548–57.
18. Mukherjee P, Uzun-Coruhlu H, Curthoys IS, Jones AS, Bradshaw AP, Pohl DV. Three-dimensional analysis of the vestibular end organs in relation to the stapes footplate and piston placement. Otol Neurotol. 2011;32(3):367–72.
19. Kaftan H, Blaurock M, Kaftan S. Design-dependent calculation of the prosthesis length in malleostapedotomy. Ann Otol Rhinol Laryngol. 2015;124(9):728–33.
20. Sudhoff H, Gehl HB, Boga E, Muller S, Wilms K, Mutze S, Todt I. Stapes prosthesis length: one size fits all?? Audiol Neurootol. 2019;24(1):1–7.
21. Kosling S, Plontke SK, Bartel S. Imaging of otosclerosis. Rofo. 2020;192(8):745–53.
22. Brucker MJ, Patel J, Sullivan PK, Department of plastic surgery BMS. Rhode Island hospital PUSA: A morphometric study of the external ear: age- and sex-related differences. Plast Reconstr Surg. 2003;112(2):647–52.
23. Zhao P, Ding H, Lv H, Li J, Liu X, Yang Z, Wang Z. Growth pattern of temporal bone pneumatization: a computed tomography study with consecutive age groups. Surg Radiol Anat. 2019;41(2):221–5.
24. Paetz P, Goetz GF, Lanfermann H, Giesemann AM. The developing temporal bone: computed tomography measurements and assessment of suture closure from birth to 18 years of age. Surg Radiol Anat. 2017;39(6):663–71.
25. Hong J, Chen K, Lyu H, Yin D, Yang L, Zhang T, Dai P. Age-related changes in the morphological relationship between the supratubal recess and the eustachian tube. Auris Nasus Larynx. 2018;45(1):88–95.
26. Almuhawas FA, Dhanasingh AE, Mitrovic D, Abdelsamad Y, Alzhrani F, Hagr A, Al Sanosi A. Age as a factor of growth in mastoid thickness and skull width. Otol Neurotol. 2020;41(5):709–14.
27. Zalewski CK. Aging of the human vestibular system. Semin Hear. 2015;36(3):175–96.
28. Ji L, Zhai S. Aging and the peripheral vestibular system. J Otol. 2018;13(4):138–40.
29. Bulygina E, Mitteroecker P, Aiello L. Ontogeny of facial dimorphism and patterns of individual development within one human population. Am J Phys Anthropol. 2006;131(3):432–43.
30. Waitzman AA, Posnick JC, Armstrong DC, Pron GE. Craniofacial skeletal measurements based on computed tomography: part II. Normal values and growth trends. Cleft Palate Craniofac J. 1992;29(2):118–28.
31. Guyader E, Savean J, Clodic C, Letellier P, Meriot P, Marianowski R. Three-dimensional reconstruction of the temporal bone: comparison of in situ, CT, and CBCT measurements. Eur Ann Otorhinolaryngol Head Neck Dis. 2018;135(6):393–8.

Publisher's note